MASTER

CONF-771136--8

PREPRINT UCRL-79772

Lawrence Livermore Laboratory

PROBLEMS WITH ρR MEASUREMENTS - WHAT ARE THE WAYS OUT?

Yu-Li Pan and Jon T. Larsen

October 25, 1977

This paper was prepared for presentation at the Nineteenth Meeting of the American Physical Society/Division of Plasma Physics, Atlanta, Georgia, November 6-11, 1977

This is a preprint of a paper intended for publication in a journal or proceedings. Since changes may be made before publication, this preprint is made available with the understanding that it will not be cited or reproduced without the permission of the author.

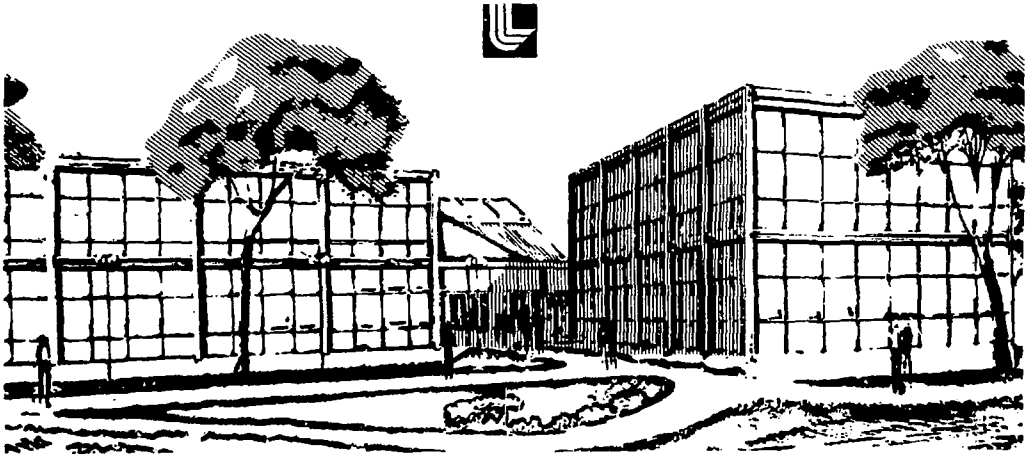

DISTRIBUTION OF THIS DOCUMENT IS UNLIMITED

PROBLEMS WITH ρR MEASUREMENTS - WHAT ARE THE WAYS OUT?*

Yu-Li Pan and Jon T. Larsen

Lawrence Livermore Laboratory
University of California
Livermore, California 94550

ABSTRACT

An important scaling parameter or figure of merit in inertially-confined fusion is the maximum fuel ρR achieved by the target - ρ is the density, and R the radius of the fuel. Every technique used, thus far, in laser-initiated-fusion-microexplosion experiments to obtain this data had major deficiencies. We examine critically the merits of the various possible methods of measuring fuel ρR and their ranges of applicability.

NOTICE

This report was prepared as an account of work sponsored by the United States Government. Neither the United States nor the United States Department of Energy, nor any of their employees, nor any of their contractors, subcontractors, or their employees, makes any warranty, express or implied, or assumes any legal liability or responsibility for the accuracy, completeness or usefulness of any information, apparatus, product or process disclosed, or represents that its use would not infringe privately owned rights.

*Work performed under the auspices of the U.S. Department of Energy under contract No. W-7405-Eng-48.

REA

OF THIS DOCUMENT IS UNLIMITED

In inertially confined fusion, the thermonuclear reaction, charged particle deposition, and electron-ion heating rates are proportional to the fuel density, ρ; the confinement time is proportional to the fuel radius, R. Therefore, the self heating, burn efficiency, and the thermonuclear burn propagation characteristics are determined by the density-radius product of the fuel, ρR. Techniques which can determine the fuel ρR unambiguously are clearly necessary.

Assuming spherical symmetry, fuel mass conservation, and uniform density, it is simple to show

$$\rho_c R_c = (\rho_o R_o^3)^{1/3} \rho_c^{2/3} \tag{1}$$

and

$$\rho_c R_c = \rho_o R_o^3 / R_c^2 \tag{2}$$

where ρ_o, ρ_c, R_o, and R_c are the initial and compressed fuel densities and radii. Thus, ρR information can be obtained indirectly by density or radius measurements. However, note that ρR depends on the compressed density, ρ_c, to the 2/3 power but the inverse square of the compressed radius, R_c. Consequently, the relative error $\frac{d(\rho_c R_c)}{\rho_c R_c} > \frac{dR_c}{R_c}$ and $\frac{d(\rho_c R_c)}{\rho_c R_c} < \frac{d\rho_c}{\rho_c}$. If other factors are negligible, to obtain a given error in ρR by the two approaches, radius measurements must have smaller

errors than density measurements. Moreover, density, being a three-dimensional quantity, is more insensitive to the influences of possible implosion asymmetries or small spatial density variations. Using radius diagnostic techniques, data must be obtained from more than a single direction to ascertain the effects of implosion asymmetries. We will discuss the details of measuring the density, radius, and ρR via different experimental techniques.

The essential discussions deal only with the various selected experimental techniques at the threshold or available conditions and not on theoretical possibilities. We have not attempted nor do we claim to have covered all the possibilities or circumstances. Weaknesses of the techniques are discussed not with the view of showing the uselessness of the method but to indicate the areas of uncertainties and/or necessary improvements. The desirability of a method, the ease of obtaining a required data, the usefulness or meaningfulness of the results depend on the particular circumstance and are to some extent subjective. Within these limits, our opinions or conclusions are influenced by our experiences and biases. The readers are encouraged to form their own opinions and conclusions according to their experiences and biases.

We find

1. Density determination using Stark broadening is difficult at low densities because of the need to isolate the Stark contribution from other line broadening mechanisms. When the Stark broadening dominates at high densities, the unfolding complications may be simpler.

2. Measurement of the compressed fuel size using x-rays emitted by the high Z microballoon is hindered by the complexities of locating the fuel-microballoon interface. Using x-rays emitted by "seed" material placed in the fuel would reduce the difficulties.

3. A 2 TW, Nd-glass laser would be required to produce the x-ray flux needed to diagnose (spatially resolved) the typical exploding-pusher, DT filled glass microballoon target experiments at 3 TW using the x-ray backlighting technique. Application of temporal and spatial resolving techniques may reduce this high laser power requirement.

4. Neutron activation technique can be used to measure the "pusher-tamper" ρR. But to determine the fuel ρR from neutron activation of the "pusher-tamper," the "pusher-tamper" should be "thin."

5. Intensity measurements of the K_α x-ray produced by the scattering of 3.5-MeV α-particles or 3 MeV protons on high Z material can be used to determine the fuel ρR. Photographic image of these K_α x-rays can also yield implosion symmetry and fuel-microballoon mixing information.

6. The extent of atomic mixing of the microballoon material into the fuel can be measured by determining the DT reaction yield degradation as a function of the Z of the microballoon material.

I. DENSITY DIAGNOSTIC

Density information can be obtained by measuring the Stark broadening of x-ray lines emitted by a tracer element of a selected atomic number placed inside of the microballoon target. This task is nontrivial because the experimentally measured width is the result of complex mixtures of several broadening components.

Within the compressed core, the line width is due to Doppler and Stark broadening.[1] The core is optically thick to the selected x-ray line radiation because of line emission intensity requirements. Opacity effects will cause additional line broadening. To obtain the observed line width and shape, the Lorentzian, Stark and the Gaussian, Doppler line shapes must be convoluted to give a Voight profile. Fine structure splitting can separate the Voight profile into two Voight profiles which are further modified by opacity effect, attenuation in the microballoon material, and the instrumental response. These effects are time varying functions of the electron temperature and density in the core and microballoon material; therefore, a steady state calculation may not be representative of the experiment. Density information can be obtained only by properly simulating the experimental conditions with a computer code like LASNEX[2] together with the time dependent calculation of the complex convolutions of the various line components.[3]

The factors governing the selection of the target and "seed" materials are outlined.

(IA) Target Material - To obtain the maximum hydrodynamic implosion efficiency, the initial density of the capsule material should be high and the x-ray background (proportional to Z^4) minimization requires that the capsule material have low Z.

(IB) "Seed" Material - Assuming that the chosen element can be placed into the target, the choice of the "seed" material is determined by the density and the fuel electron temperature achievable in the implosion.[4] The peak density should be reached when the electron temperature is above the threshold temperature for line emission and below the "burn out" temperature.

The concentration of the "seed" material is primarily determined by the line emission intensity required to overcome the x-ray background. Density, temperature, and opacity effects must also be considered. Since the compressed core is optically thick to the x-ray line emission, the x-rays observed at the spectrometer come predominately from the outer edge of the compressed core. Increasing the compressed radius by filling the target with low Z gas and a minimum amount of "seed" material will raise the x-ray line emission intensity and reduce the opacity broadening effects. Thermonuclear reaction yield measurement from the DT reaction can indicate the core ion temperature which can be used to place a limit on the Doppler line broadening contribution.[5] The low Z gas should be mixtures of D and T.

Based on these considerations, the target parameters, spectrometer resolution, and laser energy and pulse shape requirements can be obtained.

Pan and Bailey[6] have designed diagnosable DT-neon filled targets which can reach peak average-fuel-density of 1-10 g/cm^3. Diagnosable targets using DT-Ar filled microballoons which can reach peak average-fuel-density of 20 g/cm^3 have been calculated by Bailey.[4] More recently, Pan, et al.[7] have analyzed the neon-line-broadening data obtained by Auerbach, et al.[8] Their analysis demonstrates the feasibility of using the resonance line broadening technique to determine fuel density. This measurement technique is undesirable for low fuel densities because of its strong dependence on complex computer simulations and calculations. However, Bailey[4] suggests the theoretical possibility of using optically thin, higher series member line emissions to diagnose fuel densities. Complex computer simulations and theoretical interpretations may be unnecessary in this case.

II. RADIUS DIAGNOSTICS

Using radius measurements to obtain density (compression) or ρR requires good spatial resolution and simultaneous information from more than a single direction. It is illuminating to see the effect of spatial resolution on the uncertainties of density (compression) and ρR. The uncertainties are calculated by the standard differentiation technique and the "limit" method.[8a] For a target with R_0 = 50 μm, ρ_0 = 2 x 10^{-3} g/cm^3 compressed to R_c = 5 or 10 μm and diagnosed with 1 or 3 μm instrumental resolution, we obtain from Equation 2:

	ρ_c (g/cm^3)		$\rho_c R_c$ (g/cm^2)	
R_c (μm)	DIFF.	LIMIT	DIFF.	LIMIT
5±1	2.0±1.2	$2.0^{+1.9}_{-0.8}$	1.0±0.4 x 10^{-3}	$1.0^{+0.6}_{-0.3}$ x 10^{-3}
5±3	2.0±3.6	$2.0^{+29}_{-1.5}$	1.0±1.2 x 10^{-3}	$1.0^{+5.3}_{-0.6}$ x 10^{-3}
10±1	0.25±0.08	$0.25^{+0.09}_{-0.06}$	2.5±0.5 x 10^{-4}	$2.5^{+0.6}_{-0.4}$ x 10^{-4}
10±3	0.25±0.24	$0.25^{+0.48}_{-0.14}$	2.5±1.5 x 10^{-4}	$2.5^{+2.6}_{-1.0}$ x 10^{-4}

For this elementary analysis we have assumed:

(IIa) The existence of a sharp boundary between the fuel and the inside surface of the microballoon throughout the implosion (no mixing of the fuel and the microballoon material).

(IIb) The location of the fuel-balloon interface at peak compression is measured to an uncertainty of 1 or 3 μm.

(IIc) Blurring of the interface image due to motion is negligible.

(IId) The fuel-balloon interface is spherical in shape.

(IIe) Errors arising from other sources are negligible.

Under these very optimistic assumptions, we see that the uncertainties obtained from the differentiation technique in density (compression) and ρR are about 100% and 60% respectively, when the error (resolution) in R_c is 3 μm and R_c = 10 μm. Even greater errors are calculated for the 1000X compression case, where ρ_c is larger and R_c much smaller. The low compression used in the above example (125X) is similar to most implosion experiments performed to date. Using an error (resolution) in R_c of 1 μm for these cases reduces the density and ρR errors to a more reasonable level. Thus, improvements in the instrumental resolution and/or increase

in compressed size (implying larger target and laser) would be helpful in obtaining meaningful density-compression or ρR data.

All of the experiments performed to date rely on the detection of x-rays emitted or the charge particles produced by the imploding target to indicate the compressed size. These experiments have not had simultaneous information from two or more directions. The three-dimensional (3D) implosion symmetry [assumption (IId)] characteristics are uncertain. More specific comments on these two detection methods are presented below.

IIA. X-RAY

1. Existing Instruments

X-rays emitted by the high Z microballoon material have been detected with pinhole, microscope, zone plate, and spatial streak devices to yield temporally integrated and resolved spatial characteristics of the imploding targets.[9] Ignoring the effects of large instrumental resolutions and the lack of 3D implosion symmetry information,[10] the interpretations of these data depend on knowing the locations of the fuel-microballoon interface, assumptions (IIa) and (IId). Selected experiments have been simulated with the 2D, LASNEX, MHD code and good agreement has been obtained between all of the available experimental data and the computer

simulation results. In Figure 1, we show the time-space evolution of x-rays calculated by one of these target simulations for the emitted x-ray energy range of about 1.5 keV. The dotted lines in the figure represent the calculated locations of the fuel-glass interface. Peak x-ray emission does not occur at the interface, but at a radius approximately 10 μm larger. The difficulties in determining the locations of the fuel-microballoon interface from x-ray emission data are apparent.

From observing x-rays emitted from selected "seed" atoms mixed with the fuel of the target, e.g., neon, argon, the difficulties with locating the fuel-microballoon interface can, in principle, be avoided. Other uncertainties, already discussed, remain. The factors governing the selection of the target and "seed" elements for line-broadening measurements, sections (IA) and (IB), are applicable in this case.

2. Back-Lighting

X-ray radiographic technique is frequently used to produce shadowgraphs of objects. This technique for radius determination requires an external x-ray source of the proper energy and intensity.

An external x-ray source of short temporal duration timed to coincide (5-10 ps for the typical exploding-pusher targets) with the achievement of peak compression will produce a "snap-shot" picture of the imploded geometry. A short x-ray pulse can be produced by the irradiation of a

thin, flat, high-Z foil with a short intense laser pulse. To obtain the required rapid rise time in the x-ray intensity, the laser pulse must have a comparably fast rise time. The high-Z foil should be sufficiently thin so that the x-ray emission intensity is quenched quickly by hydrodynamic expansion. Figure 2 shows a LASNEX simulated x-ray temporal pulse in the 2.1-2.5 keV energy range emitted by a 50 μm diameter, 0.27 μm thick, copper foil irradiated with a 50 μm diameter spot, 1.06 μm wavelength, 15 joule, and 30 ps Gaussian laser pulse. Twenty percent of the laser energy was absorbed by the foil. Focusing the laser light to a smaller spot would reduce the amount of material heated and decrease the x-ray output.

The proper x-ray energy is determined by the desired intensity contrast produced by the spatial x-ray attenuation variation in the target material. In Figure 3, the effect of x-ray energy on the observed intensity distribution for a hollow 20 μm inside diameter, 1 μm thick spherical aluminum shell is shown. Conditions (IIa), (IIc), (IId), (IIe) are again assumed. Standard cold aluminum x-ray absorption coefficient and normal aluminum density have been used in these calculations. Using x-rays above 5 keV energy will reduce the contrast, because the absorption decreases with increasing x-ray energy. Since the aluminum absorption coefficient and density are higher than those of glass used in the typical laser fusion target, the expected contrast for glass shell will be lower than those shown in Figure 3. An instrumental resolution of less than 1 μm is necessary to detect the intensity minima shown in the figure. Increasing the absorption coefficient, density, thickness, and the size of the shell would allow poorer instrumental resolution.

An estimate of the required x-ray source intensity can be determined from the experimental x-ray spectra data obtained for typical DT filled glass microballoons irradiated at the LLL, 0.5-TW JANUS, and 3-TW ARGUS Nd-glass laser systems, Figure 4. The x-ray source should at least be equal to but preferably greater than the background intensity at the observing energy. Integrating the x-ray emission power for the distribution shown in Figure 2, the total energy is about 5×10^{14} keV/keV in the 2.1-2.5 keV range. The same LASNEX simulated experiment also produced about 5×10^{13} keV/keV in the 4.4-5.0 keV x-ray energy range. Comparisons between the calculated energy outputs and those obtained experimentally, Figure 4, show the x-ray emissions are approximately the same for the copper foil and the target irradiated at the 0.5-TW JANUS system. The x-ray output from the copper foil is at least a factor of two lower than the background produced by those target experiments using the 3-TW ARGUS system. Higher laser power would be required to produce the x-ray back-lighting source necessary to overcome the background.

Thus far, we have assumed that the x-ray background from imploding microballoons are spatially uniform. However, the x-ray energy radiated from typical glass microballoon implosions is concentrated in the compressed region especially at energies from 2 to 10 keV. Besides the need for increased x-ray back-lighting source flux (higher laser power) to overcome this more intense background, the size of the minima shown in Figure 3 can be obscured as a result and thereby create great uncertainties as to the actual location of the inner surface of the microballoon. From the above considerations, we estimate that a 2 TW, Nd-glass laser would be required to produce the x-ray back-lighting source flux needed to diagnose 3 TW target experiments.

The x-ray radiation, discussed above, can be detected with an x-ray streak camera. The need for precise timing is greatly reduced; but this advantage is neutralized by the need for a long, intense x-ray back-lighting source.

IIB. CHARGE PARTICLES

Alpha particles produced from DT reactions in the compressed cores of laser-fusion microexplosions have been imaged with pinhole and zone-plate devices.[11] The size of the reaction region can be obtained by determining the spatial distribution of the observed α-particles. A knowledge of the location of the fuel-microballoon interface is not needed. Good instrumental resolution is still necessary. The limitations or shortcomings of this method are outlined.

1. More than 10^7 DT reactions are required to produce sufficient α-particles needed by the imaging devices.

2. Since the α-particles must escape through the pusher to reach the detectors, the pusher ρR must be smaller than the range of the 3.5 MeV α-particles (less than 5×10^{-3} g/cm^2). This defines the upper limit on the applicability of the method.

3. Alpha-particle paths are changed by the strong megagauss magnetic field and large electric field known to exist in laser-initiated microexplosion experiments. For the typical glass microballoon implosions, the contributions from these effects are estimated to be smaller than the existing instrumental resolving capabilities.

4. Alpha-particle paths are altered by scattering with microballoon material. This becomes a more important consideration for high pusher ρR targets.

5. Asymmetrical compression and shock heating of the DT gas can give rise to spatial variations in the number of α-particles produced. This would create additional uncertainties in the size determination.

Protons from DD reactions can also be used to determine the size of the reaction region. This diagnostic technique suffers the same deficiencies as the α-particle method. The difference in the DT-DD reaction cross sections causes approximately 100 times fewer protons to be produced in the typical laser fusion experiments using equimolar DT filled targets. Proton background from laser heated capsule material can create further difficulties.

Using the 14.1 MeV neutrons to diagnose the size of the reaction region would alleviate most of the deficiencies of using charged particles. This requires a substantially larger DT reaction yield because of the small neutron reaction cross sections with the detector.

III. ρR DIAGNOSTICS

The quantity, ρR, has the dimensions of attenuation and appropriate measurement techniques can be used to determine ρR. The data can be obtained by particle scattering or spatial density distribution (absorption) measurement techniques. Since the requirements for the x-ray backlight technique have already been discussed, we limit our considerations of ρR diagnostics to the particle scattering method. For simplicity, we consider only the particles produced by the reactions in DT filled targets.

A DT filled microballoon target can be thought of in terms of three regions: fuel, pusher-tamper, and ablator. The pusher-tamper is defined as the inward moving portion of the microballoon which is in contact with the fuel. If we assume that the fuel and pusher-tamper masses are separately conserved, spherical symmetry, and uniform density in each of the two regions discussed, it is easy to show:

$$\frac{(\rho R)_{fc}}{(\rho R)_{fo}} = \frac{(\rho R)_{pc}}{(\rho R)_{po}} \tag{3}$$

where $(\rho R)_{fo}$, $(\rho R)_{fc}$, $(\rho R)_{po}$, $(\rho R)_{pf}$ are, respectively, the initial and compressed ρR of the fuel and pusher-tamper. Thus, in principle, the fuel ρR can be determined indirectly from pusher-tamper ρR measurements. However, the requirement of uniform pusher-tamper density restricts the applicability of the equation within narrow limits. Examination of LASNEX simulations of typical exploding-pusher targets shows that the assumption of uniform density for the inward portion of the microballoon is not satisfied.

Using $F_f = \frac{(\rho R)_{fc}}{(\rho R)_{fo}}$ and $F_p = \frac{(\rho R)_{pc}}{(\rho R)_{po}}$, the ratio of F_p/F_f as a function of assumed pusher-tamper thickness is shown in Figure 5. The curve was obtained from a LASNEX simulation for a 40 μm diameter, 0.5 μm glass microballoon target irradiated by a 40 J, 50 ps, 1.06 μm laser pulse. If we assume the pusher-tamper to be the inward moving half of the glass microballoon, F_p is only about 0.1 F_f. As the assumed pusher-tamper thickness decreases, F_p and F_f becomes more nearly equal. Thus a "thin" pusher-tamper is required to satisfy the uniform density assumption. An alternative relationship can be derived if the radial density profile of the pusher is known.

We discuss the specifics of ρR diagnostics.

IIIA. ENERGY LOSS

Time-of-flight (TOF) measurements of alpha-particles, protons, and neutrons produced in experiments using DT filled microballoons have been used to infer ion temperatures.[12] In principle, the particle energy loss measurements can also be used to determine the total target ρR. If the fuel ρR constitutes a small fraction of the total ρR, and the "pusher-tamper" is not thin, then a knowledge of the radial density profile of the shell would be required to extract meaningful fuel ρR data.

In addition to the limitations discussed in section (IIB), the temporal response characteristics of the particle detectors must be considered in TOF measurements. Typical detectors (scintillators) have fast rise but slow decay times. In order to minimize data unfolding

difficulties, the attenuated particles must be well separated in time from the "prompt" unscattered signal, usually x-rays. Reasonable counting statistics can be obtained only if a substantial fraction of the particles produced in the core interact with the target material before escaping. (For reference, the attenuation coefficient for a 14.1 MeV neutron is about 25.8 g/cm^2 in pure silicon.) The exact requirements and limitations are a function of the particles used, the target ρR, detector response characteristics, and the DT reaction yield.

IIIB. NEUTRON ACTIVATION

Neutron activation techniques have been widely used to measure the concentration of trace elements. Knowing the neutron energy, flux, activation cross section, and the initial concentration of the selected atoms, the number of activated atoms, N_a, is related to ρR according to

$$N_a = \frac{0.6\sigma}{A} (\rho R)n \qquad (4)$$

where A is the atomic weight of the material, σ is the activation cross section in barns, and n is the number of neutrons produced. The sensitivity of the method depends on several factors:

1. Cross section for the neutron reaction on the selected element and its natural abundance.
2. Detection efficiency
   a. Collection efficiency - fraction of the activated element collected for counting;

b. Delay time between activation and counting;

c. Number of decay modes;

d. Counting efficiency;

e. Background

3. Target Fabrication

The 14.1 MeV neutron activation cross sections, natural abundance, half life, and decay mode for selected elements are shown in Table I. Only those isotopes with beta decay half-lives between 1-10 minutes and elements with activation cross sections of 0.1 barn or greater are included. We discuss the use of three elements, silicon, barium, and praeseodymium to demonstrate the effects of certain constraints.

SILICON - Half of the glass by weight is silicon. The use of silicon in neutron activation analysis presents no additional problems for target fabrication. However, the activation cross section is rather low. The decay of the 2.3-minute Al^{28} proceeds by the emission of an electron whose end-point energy is 2.86 MeV followed by a 1.75 MeV gamma-ray to the stable ground state of Si^{28}. An effective way to reduce the background signal is to count the two particles in coincidence. (The half-life of the intermediate state is 0.5 ps.)

Assuming a collection efficiency of 50%, production-to-counting delay time of one half-life, coincidence counting efficiency of 10% for a period of four half-lives, without any background contribution, all the neutrons produced in the core traverse the target without any attenuation, no fuel-glass mixing, all the neutrons produced at the time of peak glass ρR, no fluid instability effects, spherical symmetry, target

ρR of 10^{-2} g/cm^2, a minimum neutron yield of about 4×10^7 is required to give 20 detectable activations.

BARIUM - Standard barium crown glass contains up to about 48% BaO by weight. Barium glass with about 70% BaO by weight can be made. With the appreciable higher activation cross section, high natural abundance, and a single decay mode, barium is, at first glance, much superior to silicon. However, Ba^{137M} decays by an isomeric transition of 0.662 MeV; hence coincidence counting techniques cannot be used to limit background.

A gross gamma-ray singles count, without spectrum analysis, can indicate the number of activated barium atoms if the signal is sufficiently greater than the background. The minimum signal required is defined to be $3\sqrt{N_b}$, where N_b is the expected background singles count. To reduce the required signal, elements which can contribute to the background should be eliminated from the target material. Assuming that special circumstances do not exist, the background for singles counting in a shielded system is typically about 100 counts/minute. Using the same assumptions as in the silicon calculation, but only counting for one half-life, a minimum neutron yield of about 1×10^8 would be required to give 30 detectable events (above background).

PRAESEODYMIUM - Pr is the ideal element from the standpoint of natural abundance and cross section. It may be difficult to fabricate Pr into a target. An additional complication arises in that there is

more than one decay mode for Pr^{140}. Fifty percent of the Pr^{140} decays to the ground state of Ce^{140} with the emission of a positron of 2.3 MeV end-point energy and 25% decays to the first excited state with the emission of a 0.72 MeV end-point energy positron followed by a 1.6 MeV gamma-ray. Applying the same assumptions as used in the silicon calculation but detecting only 25% of the Pr^{140} decay (via γ and β^+) and assume a 100% Pr concentration in the balloon, a minimum of about 4×10^7 neutrons would be required to give 20 detectable events.

From the standpoint of the minimum neutron yield requirement (about 4×10^7) for a given target ρR (1×10^{-2} g/cm^2), there is little difference in the choice of using silicon, barium or praeseodymium. However, for fuel ρR determination, there is an important difference. Using the normal material densities, the thickness of a barium or praeseodymium pusher-tamper required for a given ρR is about 5 times less than that of a silicon shell. Therefore, the required "thin" pusher-tamper for fuel ρR measurement, discussed above, can be more easily satisfied with barium or praeseodymium.

IIIC. K-SHELL X-RAY PRODUCTION

Coulomb scattering of α-particles and protons by a variety of materials have been extensively studied since the time of Rutherford. Considerable experimental K-shell x-ray production cross section by α-particles and protons are available.[13] We show, in Figure 6, the K_α x-ray production cross sections for 3.5 MeV α-particles and 3 MeV protons for targets of several atomic numbers. The excitation functions for aluminum and copper by α-particles are shown in Figure 7. Experimental

errors of less than about 10% are typical for these data. Using the known cross sections, the DT reaction yield, and initial concentration of the selected element, the number of K_α x-rays produced gives a measure of the ρR achieved. Several factors, 1. choice of material, 2. detection system, 3. signal strength required, 4. target fabrication, are now considered.

1. Material Choice

Unlike the neutron activation technique, there is great freedom in the material selection. The choice of the proper material is a compromise between the DT reaction yield, K_α x-ray production cross section, and x-ray background. Attenuation of the x-rays by the target becomes a consideration when the absorption becomes appreciable. We consider an example.

Using Figure 4, the x-ray bremsstrahlung backgrounds from the glass microballoon targets fall by about 3 orders of magnitude between 2 and 8 keV energy. The reductions become much less above 8 keV x-ray energy. Examination of Figure 6 shows the variation of the K_α x-ray production cross section has a weaker dependence on x-ray energy than the backgrounds between 2-8 keV. For maximum K_α x-ray production and minimum target background, materials emitting about 8 keV K_α x-rays are reasonable choices. Copper K_α x-ray is about 8 keV energy and copper can be used for neutron activation analysis (Table I). We select copper for further consideration.

2. Detection System

The copper K_α x-rays can be detected in a number of ways. We consider here only a system consisting of a quartz mirror and photographic

emulsion. The selection of quartz is based on its excellent resolutions and high reflection efficiencies for the $10\bar{1}0$ and $10\bar{1}\bar{1}$ planes at 8 keV. Reflection efficiencies of 63 or 78%, depending on the crystal plane used, and resolutions of about 1 eV were measured.[14]

In addition to the reflection efficiency, the detection efficiency of the system is limited by the collecting solid angle. A line focus on the emulsion with a collecting solid angle of 10^{-3} (4π) and a target-mirror separation of 3 cm, requires a cylindrical quartz mirror of 1.7 cm diameter and a radius of curvature of about 13 cm. Increasing the target-mirror spacing to 5 cm would require a mirror of about 2.7 cm diameter with a radius of curvature of about 21.8 cm. Quartz crystals of these dimensions are generally available.

A circular image of the compressed core can be obtained with a properly shaped quartz mirror. Both the intensity of the Cu K_α x-rays and its spatial distribution can be used to determine ρR. It may also be possible to observe compression asymmetries.

The photographic emulsion is the final component of the detection system. Exposure requirements for Kodak No-Screen film to obtain a diffuse density of 1.0 above Fog for 8 keV x-rays is measured to be 9×10^7 photon/cm^2.[15] This value is equivalent to a photon density of 0.9 photon/μm^2 and is easily obtainable.

3. Signal Strength

Assume that a DT filled target with a thin uniform layer of copper on the inside of the ablator region can be fabricated. The copper

K_α x-rays are obtained from the scattering of α-particles produced by DT reactions in the compressed fuel on this thin copper pusher-tamper. An estimate of the expected x-ray background is required to obtain the minimum number of copper K_α x-rays needed. Background x-rays can come from three sources.

3a. The ionization potential of copper L- and K-shell electrons are about 1.5 keV and greater than 10 keV, respectively. The peak electron temperature reached in the typical laser-fusion target experiment is much lower than 10 keV. Hence the background K_α x-rays from this source is negligible.

3b. Copper K_α x-rays can be produced by the 3 MeV DD protons. For a typical experiment using DT filled microballoons, the K_α x-ray background due to proton-copper scattering is a 10% effect.

3c. X-ray emission from the heated target material is the major contributor to the background at the copper K_α x-ray energy.

The experimental x-ray data obtained at the JANUS and ARGUS systems, Figure 4, are used to estimate the minimum DT reaction yield and ρR requirements. The results of this calculation are shown in Table II. Assumptions used are: a 3 eV line width for copper K_α x-rays, the replacement of the normal glass by CH or low Z glass, background contribution from only the compressed core, and detector collecting solid angle of 10^{-3} (4π). Further, we have defined the minimum copper K_α x-ray required to be $3\sqrt{N_b}$ where N_b is the number of background 8 keV

photons. From the known production cross section, we calculate that the minimum α-particle yields of 4×10^8 and 1×10^9 are required to diagnose a ρR of 10^{-3} g/cm^2 with a minimum statistical uncertainty of about 50% at the JANUS and ARGUS systems.[16]

The DT reaction yield of 4×10^8 is significantly above the maximum yield achieved at the JANUS system. A number of target experiments at the ARGUS facility have had yields in excess of 10^9. Therefore ρR determination by K_α x-ray production can be achieved with low Z ablator targets and existing laser systems.

4. Target Fabrication

As noted before, a DT filled target with a "thin" pusher-tamper is required for neutron activation or K-shell x-ray production ρR measurement techniques. Such double layered targets might possibly be fabricated in a number of ways.

4a. A small hole can be drilled with a laser in a microballoon. The desired material can be coated on the inside surface through this hole, and a hollow stalk attached at the hole to allow the DT filling and the sealing of the microballoon. However, for high compression targets, the imperfections introduced may cause the shell to become Rayleigh-Taylor unstable.

4b. The microballoons are produced by blowing the molten material with a blowing agent. Adding the desired element into the blow agent can give a "thin" pusher-tamper on the inside surface of the microballoon.

4c. Other techniques, e.g. ion implantation, etching, joining hemispherical sections, etc., may be satisfactory for fabricating the double-layered targets.

IIID. DIRECT FUEL ρR DETERMINATION AND MIX

Except for the line broadening technique, it has been assumed that the DT fuel is not contaminated by other materials. If the appropriate material is mixed into the fuel, the neutron activation or K-shell x-ray production methods can be used to determine the fuel ρR directly. But the activation technique would only be applicable for high fuel ρR and/or high yield targets, because of the low neutron reaction cross-sections. The calculation for the K-shell x-ray production, section IIIC, is independent of the location of the material and the results are applicable here. However, the mixing of high Z material into the DT fuel does effect the reaction yield. Figure 8 shows the neutron yield dependence on Z and concentration of seed material. Assume the "thin" pusher-tamper targets discussed in section IIIC can be fabricated, the fuel-pusher mixing effect can be determined by measuring the degradation in the neutron yield when compared to the uncontaminated target of the same dimensions.

IV. SUMMARY

Diagnosing density by resonance line-broadening measurements is feasible. The strong dependence of the technique on complex computer simulations and theoretical interpretations greatly increases the uncertainties of the results at low densities. But this undesirable feature can, in principle, be avoided when the Stark broadening contribution dominates at high densities.

Radius measurements can be used, in principle, to determine density or ρR. Good instrumental resolution, and a knowledge of the location as well as the shape of the fuel-microballoon interface are required to obtain meaningful results.

Neutron activation technique can be used to measure the "pusher-tamper" ρR. But a "thin" "pusher-tamper" is required for fuel ρR determination.

Intensity measurements of the K-shell x-rays produced by the Coulomb scattering of α-particles and protons on high Z material can give indirect fuel ρR information. Spatial variations in the x-ray production can be used to determine the implosion symmetry. Low Z ablator targets would be essential.

Mixing the appropriate elements into the DT fuel may make the direct fuel ρR measurement with neutron activation of K-shell x-ray production techniques possible. But DT reaction yield degradation occurs with high Z material contamination.

ACKNOWLEDGMENTS

Discussions with D. S. Bailey, N. M. Ceglio, C. W. Hatcher, C. D. Hendricks, L. N. Koppel, R. A. Lerche, J. Nuckolls, J. G. Rittmann, V. W. Slivinsky, and J. J. Thomson were beneficial.

TABLE I.

NEUTRON ACTIVATION PARAMETERS

Reaction	Decay Time	% Nat. Abundance	14.1 MeV Reaction Cross Section	Decay Mode
$Si^{28}(n,p)Al^{28}$	2.31 min	92.21	0.2 barn	β^-
$P^{31}(n,\alpha)Al^{28}$	2.31 min	100	0.1	β^-
$Cr^{52}(n,p)V^{52}$	3.77 min	83.76	0.1	β^-
$Cu^{63}(n,2n)Cu^{62}$	9.90 min	69.09	0.5	β^+, EC
$Br^{79}(n,2n)Br^{78}$	6.50 min	50.54	0.8	β^+, EC
$Rb^{87}(n,2n^*)Rb^{86M}$	1.04 min	27.85	0.6	IT
$Pd^{104}(n,p^*)Rh^{104M}$	4.41 min	10.97	0.1	IT, β^-
$Pd^{110}(n,2n^*)Pd^{109M}$	4.70 min	11.81	1.0	IT
$Ag^{109}(n,2n)Ag^{108}$	2.42 min	48.18	0.9	β^-, β^+, EC
$In^{115}(n,2n)In^{114}$	1.20 min	95.72	0.4	β^-, β^+, EC
$Sb^{123}(n,2n^*)Sb^{122M}$	4.20 min	42.75	1.3	IT
$Te^{128}(n,\alpha^*)Sn^{125M}$	9.70 min	31.79	0.4	β^-
$Ba^{137}(n,n^*)Ba^{137M}$	2.55 min	11.32] 82.98	0.3] 0.9	IT
$Ba^{138}(n,2n^*)Ba^{137M}$	2.55 min	71.66]	1.2]	IT
$Pr^{141}(n,2n)Pr^{140}$	3.39 min	100	1.8	EC, β^+
$Nd^{142}(n,2n^*)Nd^{141M}$	1.05 min	27.11	0.7	IT
$Sm^{144}(n,2n)Sm^{143}$	8.90 min	3.09	0.7	EC, β^+
$Sm^{144}(n,2n^*)Sm^{143M}$	1.01 min	3.09	0.7	IT
$W^{180}(n,2n^*)W^{179M}$	5.20 min	0.14	0.4	IT

TABLE II.

COPPER K_α X-RAY PRODUCTION REQUIREMENTS

	JANUS (0.5 TW)	ARGUS (3 TW)
Background - 8 keV glass microballoon	10^{11} keV/keV	10^{12} keV/keV
K_α line width - 3 eV	3×10^{8} keV/3 eV	3×10^{9} keV/3 eV
CH or low Z glass	3×10^{6} keV/3 eV	3×10^{7} keV/3 eV
Background in compressed core	1.5×10^{6} keV/3 eV	1.5×10^{7} keV/3 eV
Number of 8 keV photons	2×10^{5} photon/3 eV	2×10^{6} photon/3 eV
10^{-3} (4π) solid angle, N_b	2×10^{2} photon/3 eV	2×10^{3} photon/3 eV
Minimum number ($3\sqrt{N_b}$) of Cu, K_α x-ray required in 10^{-3} (4π) solid angle	40	130
Minimum DT reaction yield from the target	4×10^{8}	1×10^{9}

FOOTNOTES AND REFERENCES

1. Fuel mass motion can increase the Doppler broadening. Because of the large optical depth in the core for the x-ray line emission, only the red shift component would be observed during the implosion phase and the blue shift component, during the explosion phase of the compression experiment. Since the temperature, density, and attenuations are time varying, the contributions from the red and blue shift components can be unequal. Therefore, the observed line shape may not be symmetrical. The effect of Doppler broadening due to mass motion should be negligible if the target is properly designed and the experiment correctly performed.

2. G. B. Zimmerman, Lawrence Livermore Laboratory Report UCRL-75173 (1973).

3. D. S. Bailey and E. Valeo, Bull. Amer. Phys. Soc. 21, 1134 (1976); Lawrence Livermore Laboratory Report UCRL-78473 (1976); D. S. Bailey, Lawrence Livermore Laboratory Laser Program Annual Report-1976, UCRL-50021-76 (1977).

4. D. S. Bailey, Bull. Amer. Phys. Soc. October, 1977, to be presented at American Physical Society Meeting, Atlanta, Georgia, November, 1977.

5. Limits on the electron temperature can also be found from the presence or absence of known x-ray line emissions from the selected atoms.

6. Y. L. Pan and D. S. Bailey, Bull. Amer. Phys. Soc. 21, 1134 (1976); Lawrence Livermore Laboratory Report UCRL-78472 (1976); Y. Pan, Lawrence Livermore Laboratory Laser Program Annual Report-1976, UCRL-50021-76 (1977).

7. Y. L. Pan, D. S. Bailey, and J. J. Thomson, Lawrence Livermore Laboratory Laser Program Annual Report-1976, UCRL-50021-76 (1977).

8. J. Auerbach, et. al., Lawrence Livermore Laboratory Laser Program Annual Report-1976, UCRL-50021-76 (1977).

8a. When the uncertainties in a physical parameter become significant compared to the value itself, the results from different error calculation methods diverge. Using the standard differentiation technique, one obtains symmetrical errors which may become unphysical at the low-side.

With the "limit" method, the errors can be calculated using the measured value increased or decreased by the measurement errors. To obtain the errors on the density, ρ_c, for example, density and its errors would be calculated using R_c+dR_c, R_c, and R_c-dR_c. The "limit" method, in the cases considered here, invariably calculates small low-side and large high-side errors yielding an unsymmetrical error distribution which is not easily usable in error propagation calculations. Further, it tends to convey and propagate the dangerous and erroneous notion that errors are limits which can't be broached instead of probabilities.

We do not care to dwell on the fact that the errors are different, especially, when the difference is smaller than the error. To us, an 80-90% error is not significantly different from a 100% error. Nor do we feel it worthwhile to consider the difference between a zero and nearly zero value when the error in the parameter is larger. Since the simple error calculations performed here consider only the contribution from a single parameter in a multi-parameter space, these one-parameter differences become even more insignificant when a complete error

calculation is performed. We prefer to note that the errors are too large and focus our attention on the more important question on how to reduce the large errors so as to avoid the above difficulties.

9. See for example: x-ray pinhole - P. M. Campbell, G. Charatis, and G. R. Montry, Phys. Rev. Lett. 34, 74 (1975); x-ray microscope - F. Seward, J. D. Dent, M. J. Boyle, L. N. Koppel, T. L. Harper, J. P. Stoering, and A. Torr, Rev. Sci. Instrum. 47, 464 (1976); streak camera - D. T. Attwood, L. W. Coleman, M. J. Boyle, J. T. Larsen, D. W. Phillion, and K. R. Manes, Phys. Rev. Lett. 38, 282 (1977); zone plate - N. M. Ceglio, Proc. SPIE, 106, 55 (1977).

10. A zone plate can be used to obtain three dimensional compression geometry. The transverse resolution is determined by the zone spacing and the tomographic resolution is set by the number of zones as well as the size of the zone plate. Present fabrication constraints limit the possible transverse and tomographic resolutions to about 3 μm and 10 μm, respectively.

11. V. W. Slivinsky, K. M. Brooks, H. G. Ahlstrom, E. K. Storm, H. N. Kornblum, and G. R. Leipelt, Appl. Phys. Lett. 30, 555 (1977); N. M. Ceglio and L. W. Coleman, Phys. Rev. Lett. 39, 20 (1977).

12. V. W. Slivinsky, H. G. Ahlstrom, K. G. Tirsell, J. Larsen, S. Glaros, G. B. Zimmerman, and H. Shay, Phys. Rev. Lett. 35, 1083 (1975); R. A. Lerche, L. W. Coleman, J. W. Houghton,

D. R. Speck, and E. K. Storm, Appl. Phys. Lett., to appear in November 15, 1977.

13. See the following review paper for references: J. D. Garcia, Rev. Mod. Phys. 45, 111 (1973).

14. G. Brogren, Arkiv Fysik 22, 267 (1962).

15. C. M. Dozier, D. B. Brown, L. S. Birks, P. B. Lyons, and R. F. Benjamin, Naval Research Laboratory, Preprint August, 1976.

16. A ρR of 10^{-3} g/cm^2 is used because of the small range of the alpha-particles.

FIGURE CAPTIONS

1. Time-space evolution of x-ray emission from exploding-pusher glass microballoon target as simulated by LASNEX. The dotted lines represent the location of the fuel-glass interface.

2. LASNEX simulated temporal x-ray emission pulse shape for a copper foil irradiated by a 1.06 μm laser pulse.

3. Transmitted x-ray intensities for an aluminum spherical shell using 2 and 5 keV x-ray energies.

4. Experimental x-ray spectra for glass microballoon targets irradiated by the 0.5 TW, JANUS and 3 TW, ARGUS laser systems.

5. The ratio, F_p/F_f vs. assumed pusher-tamper thickness for a LASNEX simulated glass microballoon target.

6. Experimental K_α x-ray production cross sections.

7. Experimental K_α excitation functions for aluminum and copper using alpha-particles.

8. LASNEX simulated neutron yield as a function of the concentration and Z of the doping material.

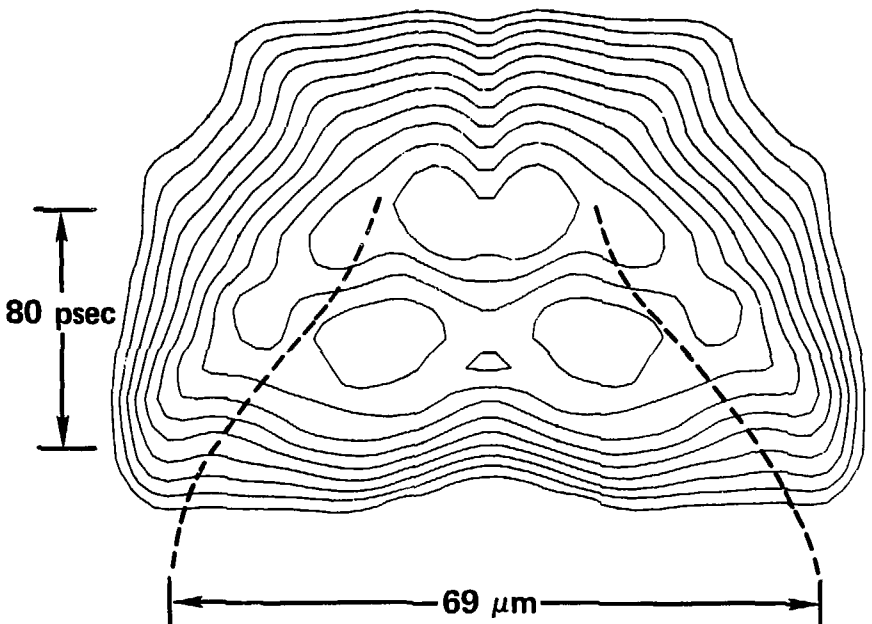

Figure 1

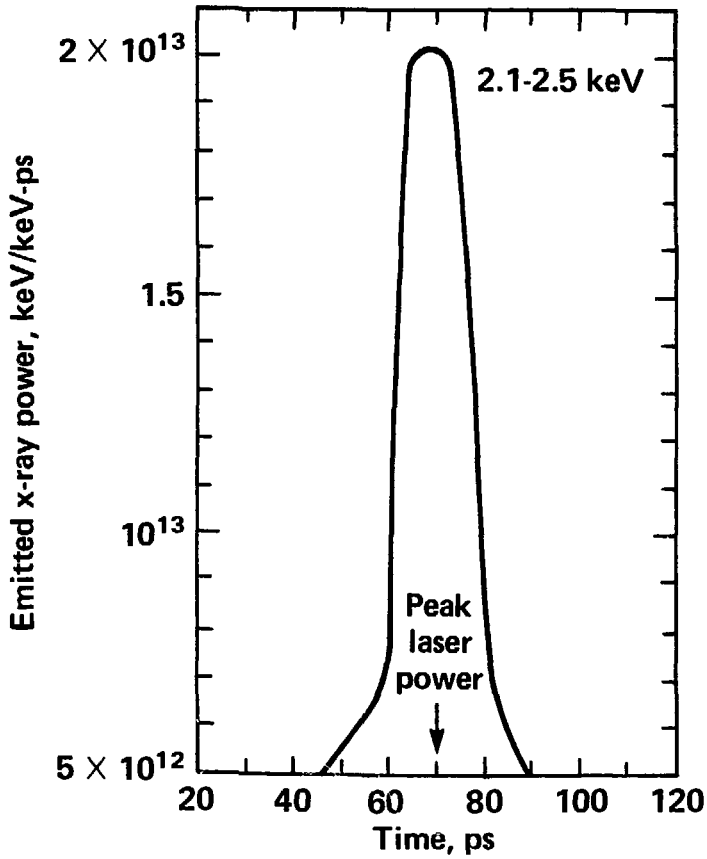
2 × 10^13
1.5
10^13
5 × 10^12
Emitted x-ray power, keV/keV-ps
2.1-2.5 keV
Peak
laser
power
20
40
60
80
100
120
Time, ps

Figure 2

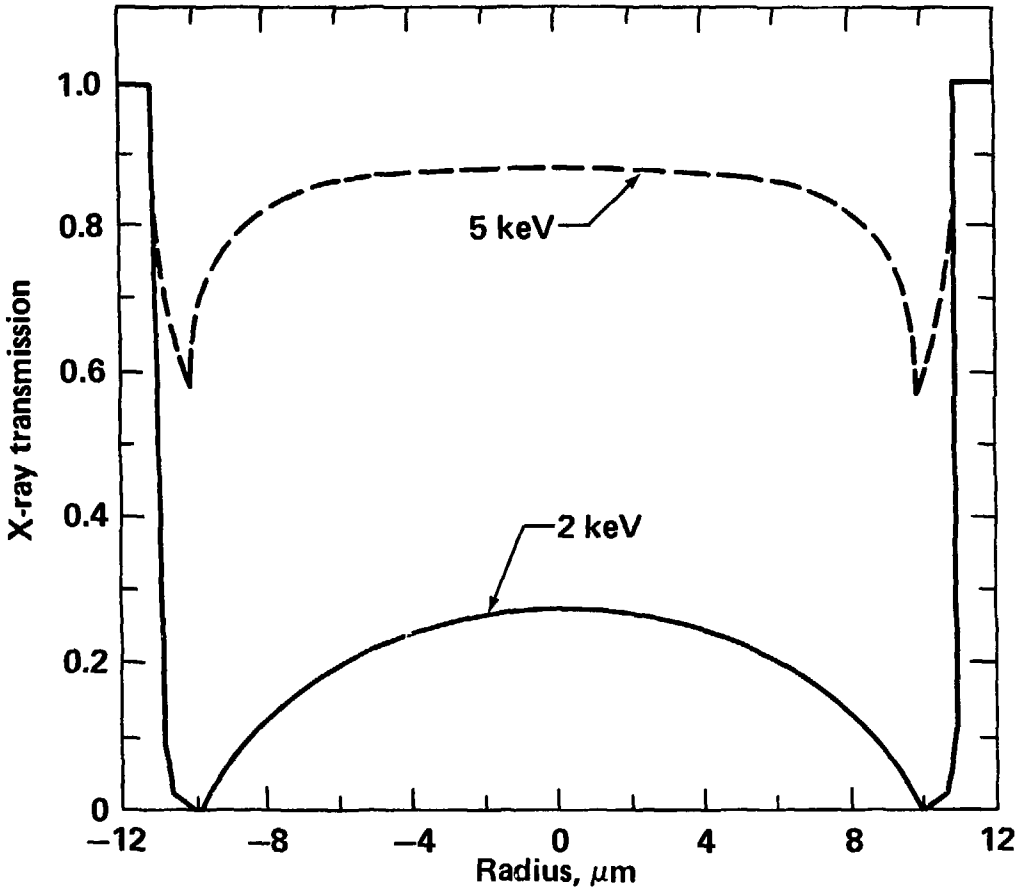
1.0
0.8
0.6
0.4
0.2
0
X-ray transmission
5 keV
2 keV
−12
−8
−4
0
4
8
12
Radius, μm

Figure 3

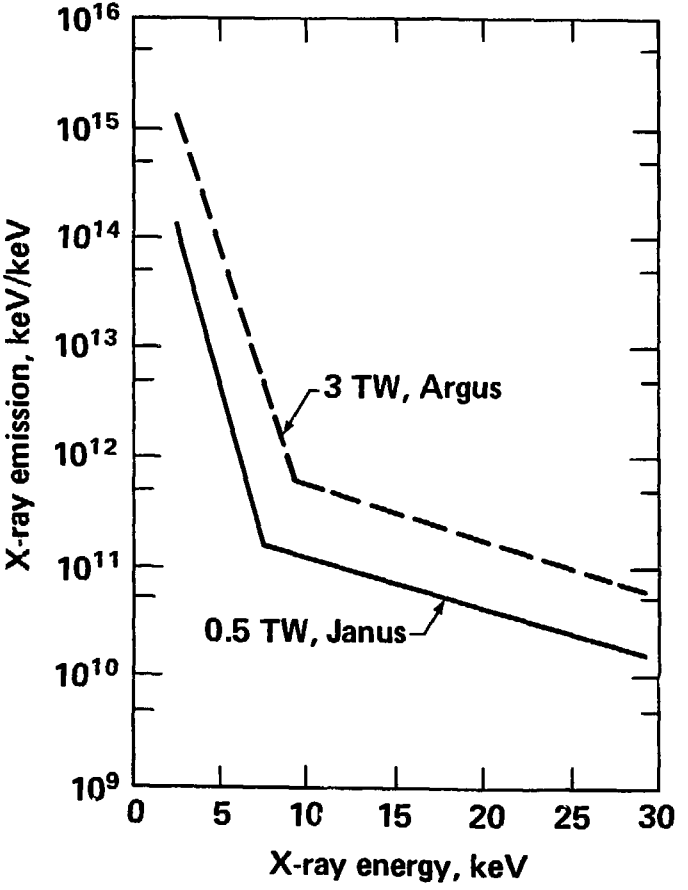
10^{16}
10^{15}
10^{14}
10^{13}
10^{12}
10^{11}
10^{10}
10^{9}
X-ray emission, keV/keV
3 TW, Argus
0.5 TW, Janus
0
5
10
15
20
25
30
X-ray energy, keV

Figure 4

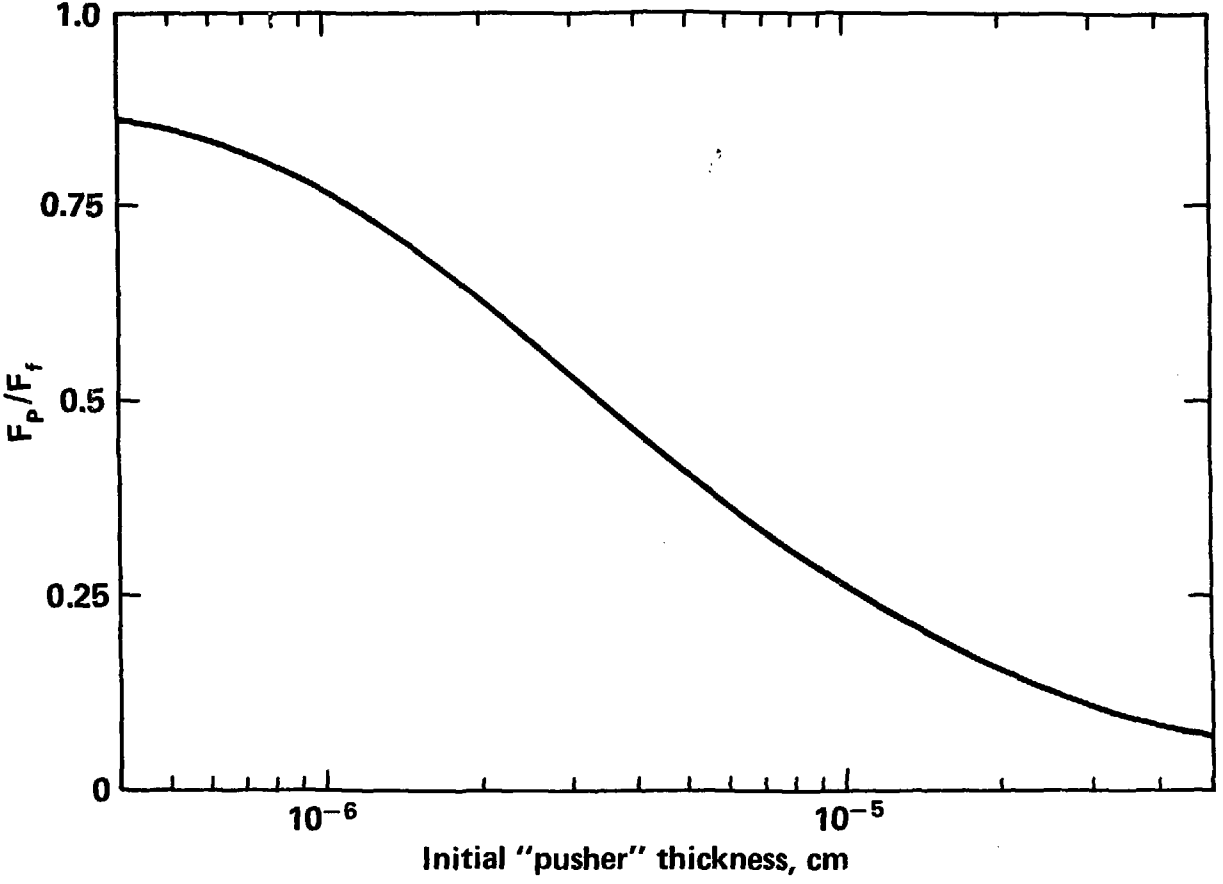

Figure 5

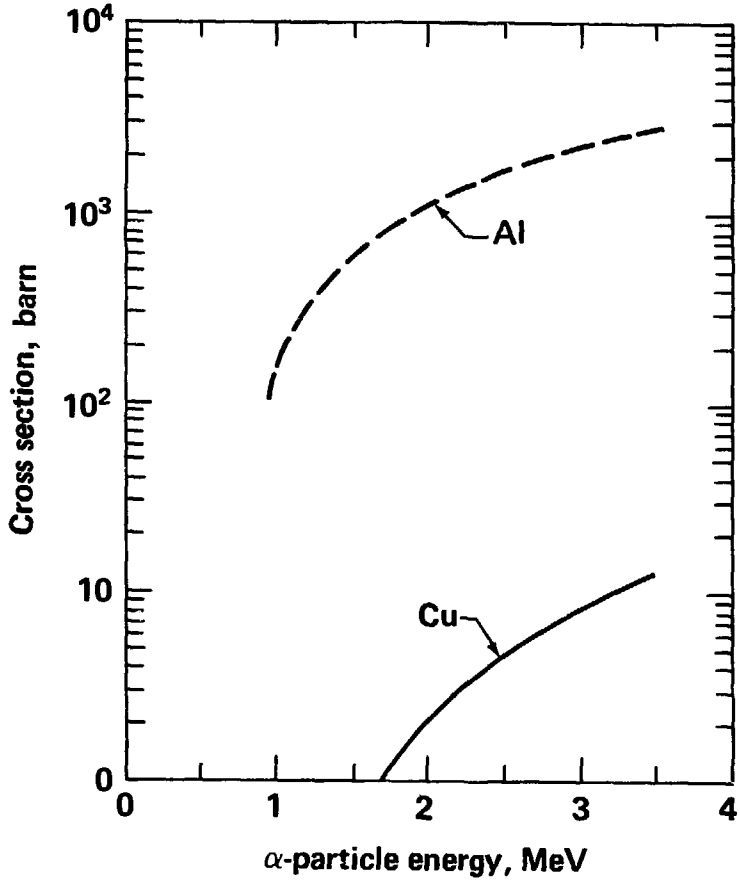
10^4
10^3
10^2
10
0
Cross section, barn
Al
Cu
0
1
2
3
4
α-particle energy, MeV

Figure 7

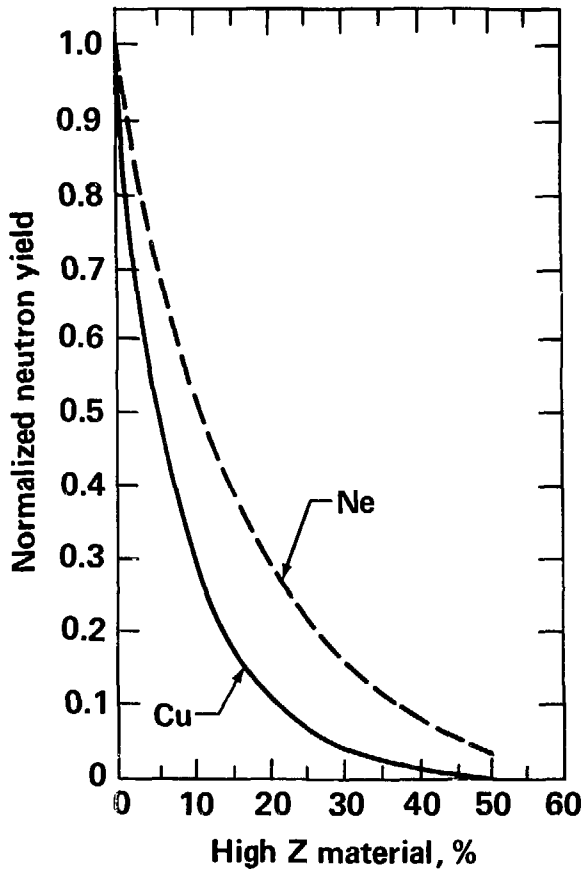
Normalized neutron yield
1.0
0.9
0.8
0.7
0.6
0.5
0.4
0.3
0.2
0.1
0
0
10
20
30
40
50
60
High Z material, %
Ne
Cu

Figure 8